



Thermodynamic modeling, material selection, and new dimensioning of a multilayer regenerator for a magnetic refrigeration system

Zina Meddeb¹

Received: 26 December 2022 / Accepted: 13 July 2023 / Published online: 18 August 2023
© Akadémiai Kiadó, Budapest, Hungary 2023

Abstract

The present work aimed to model magnetic entropy and deduce the magnetocaloric effect of materials for different temperature ranges. This modeling was based on thermodynamic and statistical approaches. Five expressions of magnetic entropy for temperatures far below, below, equal to, above, and far above the Curie temperature (T_c) were determined. Comparison with experimental values shows that three models for temperatures far below, above, and far above T_c are valid. For temperatures below T_c , we verified that a semi-empirical equation was the most appropriate. And for temperatures such as $T \cong T_c$, a theoretical model—the Oesterreicher and Parker equation—is the most appropriate, provided that the T_c of the material is close to room temperature and the magnetic field is relatively low. The exploitation of these models and their substitutions in other theoretical equations allowed us to determine the maximum magnetocaloric effect and the T_c of $Gd_\alpha R_{(1-\alpha)}$ alloys as a function of gadolinium α concentration. Based on these parameter models, which are the most pertinent for a magnetic regenerator, we developed a new method for choosing the right material to use in a magnetic refrigeration system and presented its flowchart. Finally, an original method for sizing a multilayer magnetic refrigeration system, which takes into account thermal, fluidic, and calorimetric properties and thermodynamic cycles according to a given specification, is detailed, and its steps are presented in a flowchart.

Keywords Magnetic entropy · Magnetocaloric effect · Magnetic refrigeration · Paramagnetic materials · Active material selection · Multilayer regenerator · Dimensioning method

List of symbols

B	Magnetic induction (T)	MCE	Magnetocaloric effect (–)
$B_J(x)$	Brillouin function (–)	N_{layer}	Number of layers (–)
C	Curie constant (–)	P	Pressure (Pa)
C_B	Specific heat at constant field ($J\text{ kg}^{-1}\text{ K}^{-1}$)	S	Entropy ($J\text{ K}^{-1}$)
C_p	Specific heat at constant pressure ($J\text{ kg}^{-1}\text{ K}^{-1}$)	S_r	Lattice entropy ($J\text{ kg}^{-1}\text{ K}^{-1}$)
e	Thickness (m)	S_m	Magnetic entropy ($J\text{ kg}^{-1}\text{ K}^{-1}$)
F	Faraday's constant/free energy ($-J$)	ΔS_m	Variation of magnetic entropy ($J\text{ kg}^{-1}\text{ K}^{-1}$)
G	Free enthalpy (J)	T_c	Curie temperature of a material (K)
g	Lander factor (–)	T_m	Material temperature (K)
H	Enthalpy (J)	ΔT_{ad}	Magnetocaloric effect (–)
J	Angular momentum ($\text{kg m}^2\text{ s}^{-1}$)	V	Volume (m^3)
k_B	Boltzmann's constant	Z	Partition function (–)
Lm	Regenerator length (m)		
M	Magnetization ($A\text{ m}^{-1}$)	Greek letters	
m	Mass (kg)	α	Alloy concentration (–)
		μ_B	Magnetic permeability ($H\text{ m}^{-1}$)
		χ_m	Magnetic susceptibility ($H\text{ m}^{-1}$)

✉ Zina Meddeb
zinameddeb1@gmail.com

¹ University of Gabes, National School of Engineers, Gabes, Tunisia

Introduction

The proportion of energy consumption and greenhouse gas (GHG) emissions generated by domestic and industrial refrigeration and air-conditioning applications continues to soar worldwide. This energy consumption is likely to increase rapidly due to global warming. Current environmental requirements and green standards limit conventional technologies, particularly thermodynamic techniques based on the compression–expansion cycle of gases (such as CFCs and HCFCs) [1–3]. Research into future refrigeration technologies is moving toward other principles, such as magnetocaloric refrigeration, whose advantages include zero GHG emissions, silent operation, and high efficiency [4]. Another fundamental benefit is that magnetic refrigeration can reach very low temperatures if the operating parameters are well chosen. In particular, this type of refrigeration can be used to liquefy hydrogen, which has a condensation temperature of around 22 K at atmospheric pressure, or any other cryogenic uses that are impossible with conventional refrigeration systems.

All magnetic refrigeration technologies use properties and physical phenomena specific to materials resulting from the application of a magnetic field. Applying a magnetic field to a material causes the spins to orient themselves in a specific direction resulting in a reduction in disorder and, thus, in magnetic entropy (ΔS_m). Also, reducing the magnetic field causes the opposite phenomenon, i.e., an increase in magnetic entropy. In an adiabatic process, the change in total entropy (ΔS), the sum of the change in magnetic entropy, and the change in lattice

entropy (ΔS_r) is zero ($\Delta S = \Delta S_m + \Delta S_r = 0$, the electron entropy is neglected). Therefore, any decrease in ΔS_m is offset by an increase in ΔS_r , and vice versa. The increase in a material's ΔS_r is due to the increased agitation of its molecules, which in turn implies an increase in the material's temperature. The decrease in ΔS_r is due to the decrease in the agitation of the molecules, which in turn leads to a decrease in the material's temperature. The magnetocaloric effect can, therefore, be summed up by the fact that the application of a magnetic field aligns the magnetic moments, creating a form of order in a magnetocaloric material. Under adiabatic conditions and for paramagnetic or ferromagnetic materials, this transition from a disordered magnetic state to an ordered one is accompanied by an increase in the intensity of atomic vibrations, raising the temperature in the material. Decreasing the magnetic field causes the opposite phenomenon, i.e., a decrease in temperature. [5–8].

The magnetocaloric effect is only noticeable at temperatures very close to the material's Curie temperature (T_c) (the critical transition temperature between the ferromagnetic and paramagnetic phases). Figure 1b shows that the T_c changes if the active material changes [9]. Figure 1a shows that the variation of magnetic entropy increases considerably as a function of the applied magnetic field; this variation is maximal at the T_c but lower on either side of the T_c temperature [10].

The response of a magnetocaloric material to a magnetic field (magnetization and demagnetization) is similar to the reaction of gas to compression or expansion replaced by magnetization (heating) and demagnetization (cooling), respectively. The direct exploitation of the magnetocaloric

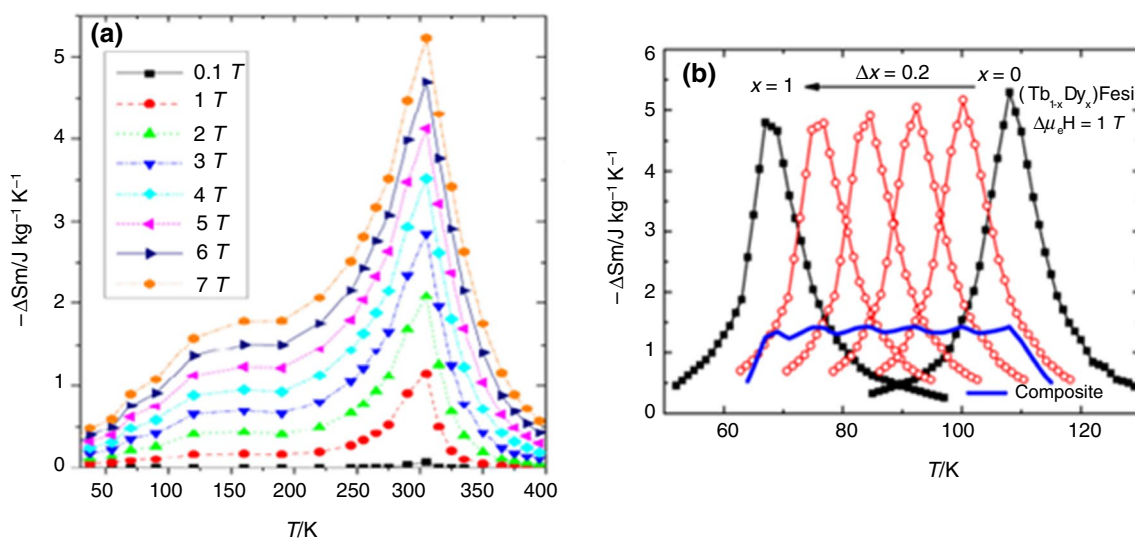


Fig. 1 **a** Magnetic entropy changes in the $\text{Gd}_{0.4}\text{Tb}_{0.6}\text{Co}_2$ as a function of temperature and magnetic field [10] **b** Temperature dependence of magnetic entropy for $(\text{Tb}_{1-x}\text{Dy}_x)\text{FeSi}$ ($x=0-1$) compounds and the composite material under a magnetic field of 1 T [9].

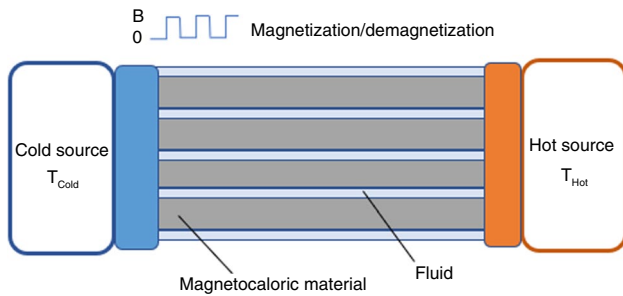


Fig. 2 Schematic representation of an active magnetic regenerative refrigeration system

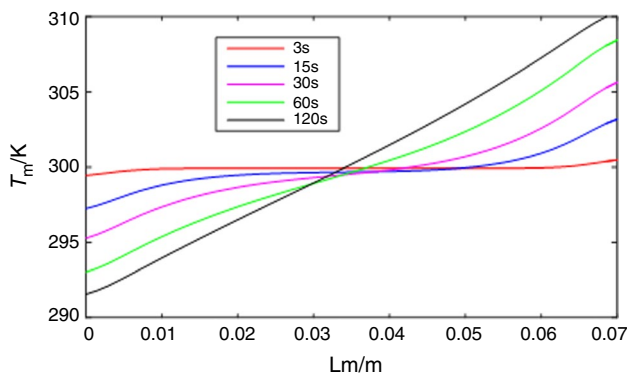


Fig. 3 Temperature variation along the length of the active material between cold and hot sides.

effect around the material's transition temperature is limited because existing magnetocaloric materials are unable to achieve high temperature differentials. This technical barrier can be overcome by applying active magnetic regenerative cooling [11]. Figure 2 gives a schematic presentation of an active magnetic regenerative refrigeration system. The four stages of this cycle are as follows:

Step 1 Material magnetization. The entire system is at an initial temperature. The temperature of each point of the regenerator material increases by ΔT .

Stage 2 Fluid flows from cold source to hot source. The heat of magnetization is dissipated by the fluid flowing from the cold source to the hot one. A temperature gradient is created along the bed.

Stage 3 Material demagnetization. The temperature at each point of the regenerator drops by ΔT as a result of demagnetization.

Stage 4 Fluid flows from the hot source to the cold source. The fluid flowing from the hot source to the cold one transfers its heat to the regenerator. The gradient is amplified.

Based on a previous study [12] and the resolution of the continuity, momentum, and energy conservation equations [13–18], we determined the temperature profile along the active material. Figure 3 shows the profile found by numerical simulation, where the material is gadolinium, the heat transfer fluid is water, the pressure is atmospheric, and the temperature difference between the hot and cold sides is 20. The temperature profile is not constant along the entire material's length, and after a transient, the material temperature profile is almost linear between the cold and hot sides. If the temperature gap between the hot and cold sides is large, a multi-layer regenerator is required since the magnetocaloric effect only manifests at the T_c of the material used.

Improvements in heat transfer between the regenerator (active material) and the heat transfer fluid are possible using nanofluids [19–26]. To master this technology and increase its efficiency, we need to control the parameters on which the value of the regenerator's magnetocaloric effect depends, including the material's T_c , the applied magnetic field, and the material's mass (since entropy is an extensive quantity).

These quantities are generally determined experimentally by characterizing the materials, and a database can be built from them, but the exploitation of this database is difficult because it is random. However, we can find some theoretical models to predict the thermodynamic properties of the material [27]; However, these models are rare and still in differential form. A model of these quantities is therefore necessary for their subsequent use. Extensive research has been carried out worldwide to develop promising magnetocaloric refrigeration technologies, which have enabled us to understand the mechanisms of the magnetocaloric effect exhibited by many materials and to manufacture new alloys likely to be used massively for refrigeration and air conditioning in the years to come. A summary of recent advances in materials development and the development of magnetocaloric cooling and heating prototypes shows that there are no methods for sizing a magnetic refrigeration system.

Our work is part of an effort to highlight the importance of an optimized design of the magnetocaloric regenerators at the heart of these machines. In this work, theoretical approaches were developed, validated, and exploited to find original models and methods for choosing the appropriate magnetic material to use according to well-defined specifications. A method for sizing a multi-layer magnetic regenerator will then be developed.

Theoretical modeling

Before presenting the theoretical modeling of magnetic entropy, we introduce the thermodynamic and statistical approaches.

Thermodynamic approach

The differential of the free energy F [28, 30] is:

$$dF(V, B, T) = -PdV - MdB - SdT \quad (1)$$

The material is solid, so there is no change in volume, hence:

$$dF(B, T) = -MdB - SdT \quad (2)$$

So,

$$M = -\left(\frac{\partial F}{\partial B}\right)_T \quad (3)$$

$F(B, T)$ is a state function; therefore, its differential is an exact total differential. Thus, we can write:

$$\Delta S_m(T, B) = \int_0^B \left(\frac{\partial M}{\partial T}\right)_B dB \quad (4)$$

Statistical approach

The free energy of the system, made up of N magnetic atoms, has the following form [31–35]

$$F = -Nk_B T \ln Z \quad (5)$$

N is the Avogadro number, k_B is Boltzmann's constant, and Z is the partition function.

The statistical sum (partition function) of a system can be determined as follows:

$$Z = \frac{\sinh(2J+1)\frac{x}{2}}{\sinh\left(\frac{x}{2}\right)} \quad (6)$$

with

$$x = \frac{J\mu_B g B}{k_B T} \quad (7)$$

where g is the Landé factor, and J is the total angular momentum.

The free energy of the system is therefore as follows:

$$F = -Nk_B T \ln \left(\frac{\sinh(2J+1)\frac{x}{2}}{\sinh\left(\frac{x}{2}\right)} \right) \quad (8)$$

We can write:

$$M = NJg\mu_B B_J(x) \quad (9)$$

where $B_J(x)$ is the Brillouin function given by the following equation:

$$B_J(x) = \frac{2J+1}{2J} \coth\left(\frac{2J+1}{2J}x\right) - \frac{1}{2J} \coth\frac{x}{2J} \quad (10)$$

Theoretical modeling of magnetic entropy

The Curie temperature, or critical temperature (T_c), is the temperature at which magnetic materials undergo a sudden change in their magnetic properties. It is considered the critical point at which a material's intrinsic magnetic moments change direction. An abrupt change in the magnetic properties of materials occurs when the magnetic phase changes.

For each interval of variation of x , we can approximate the Brillouin function $B_J(x)$ and then deduce the expression of the magnetic entropy.

- For $x \ll 1$ ($T \gg T_c$).

For this temperature range, we can write that:

$$B_J(x) = \frac{x(J+1)}{3J} \quad (11)$$

So, from Eqs. 4 and 12, we can write that:

$$\Delta S_m = \frac{-N(g\mu_B)^2 (J+1)JB^2}{6KT^2} \quad (12)$$

- For $x \gg 1$ ($T \ll T_c$).

The Brillouin function $B_J(x)$ is:

$$B_J(x) \cong 1 - \frac{1}{J} e^{-\frac{x}{J}} \quad (13)$$

And after all the calculations, we find:

$$\Delta S_m = \left(\frac{Ng\mu_B B}{T} + k_B N \right) \left(e^{\frac{-g\mu_B B}{k_B T}} - 1 \right) \quad (14)$$

- For $T \cong T_c$

Oesterreicher and Parker [29, 35] give the following equation for ΔS_m for a ferromagnetic material whose temperature is close to its T_c .

$$\Delta S_m = -1.07 N k_B \left(\frac{g \mu_B J B}{k_B T_c} \right)^{2/3} \quad (15)$$

- For $T > T_c$

Curie–Weiss law [7] gives the following expression:

$$\frac{1}{\chi_m} = \frac{T - T_c}{C} \quad (16)$$

with χ_m is the magnetic susceptibility, and C is the Curie constant:

$$C = \frac{N g^2 \mu_B^2 \mu_0 J(J+1)}{3 k_B} \quad (17)$$

Indeed,

$$M = \chi_m \frac{B}{\mu_0} \quad (18)$$

So,

$$M = \frac{N g^2 \mu_B^2 J(J+1)}{3 k_B (T - T_c)} B \quad (19)$$

The variation of magnetization with temperature at constant B is:

$$\frac{dM}{dT} = - \frac{N g^2 \mu_B^2 J(J+1)}{3 k_B (T - T_c)^2} B \quad (20)$$

Therefore,

$$\Delta S_m = - \int_0^B \frac{N g^2 \mu_B^2 J(J+1)}{3 k_B (T - T_c)^2} B dB \quad (21)$$

After integration, we find:

$$\Delta S_m = - \frac{N g^2 \mu_B^2 J(J+1) B^2}{6 k_B (T - T_c)^2} \quad (22)$$

Theoretical modeling of the magnetocaloric effect

The total differential of entropy is also exact since it is a state function, so:

$$\frac{C_p}{T} = \left(\frac{\partial S}{\partial T} \right)_B \quad (23)$$

For an adiabatic transformation, we can write:

$$dT = - \frac{T}{C_p} \left(\frac{\partial S}{\partial B} \right)_T dB \quad (24)$$

Under such conditions, the magnetocaloric effect for an adiabatic transformation ($\Delta T_{ad}(T, B)$) can be calculated using the formula below:

$$\Delta T_{ad}(T, B) = - \frac{T \Delta S_m(T, B)}{C_p} \quad (25)$$

Consequently, it is sufficient to determine the magnetic entropy to deduce $\Delta T_{ad}(T, B)$.

Theoretical modeling of the Curie temperature

The material to be used is active at its T_c . For example, when designing a magnetic refrigeration system, we need to choose a material with a T_c close to its operating temperature. Considering a Gd alloy $R\alpha(1-\alpha)$, where α is the concentration of Gd, we can write the following relationships [37–41]:

$$m_{Gd_\alpha R_{(1-\alpha)}} = \alpha m_{Gd} + (1 - \alpha) m_R \quad (26)$$

$$\mu_{Gd_\alpha R_{(1-\alpha)}}^2 = \alpha \mu_{Gd}^2 + (1 - \alpha) \mu_R^2 \quad (27)$$

m is the molecular mass.

The effective magnetic moment μ can be calculated by:

$$\mu = g \sqrt{J(J+1)} \quad (28)$$

Furthermore, the T_c of alloys obeys the empirical law established by P. Gilles Gennes [34] evaluated as:

$$G_{Gd_\alpha R_{(1-\alpha)}} = \alpha G_{Gd} + (1 - \alpha) G_R \quad (29)$$

$$G = (g - 1)^2 J(J + 1) \quad (30)$$

where G is the de Gennes factor

The Landé g -factor $g_{Gd_\alpha R_{(1-\alpha)}}$ and the total angular momentum $J_{Gd_\alpha R_{(1-\alpha)}}$ are given by:

$$g_{Gd_\alpha R_{(1-\alpha)}} = \frac{\mu_{Gd_\alpha R_{(1-\alpha)}}}{\mu_{Gd_\alpha R_{(1-\alpha)}} - \sqrt{G_{Gd_\alpha R_{(1-\alpha)}}}} \quad (31)$$

$$J_{Gd_\alpha R_{(1-\alpha)}} = \frac{1}{2} \left(\sqrt{1 + \left(\frac{2 \mu_{Gd_\alpha R_{(1-\alpha)}}}{g_{Gd_\alpha R_{(1-\alpha)}}} \right)^2} - 1 \right) \quad (32)$$

Knowing that the T_c is calculated by the following relationship [34]:

Fig. 4 Comparison of theoretical and experimental values of magnetic entropy as a function of temperature (gadolinium)

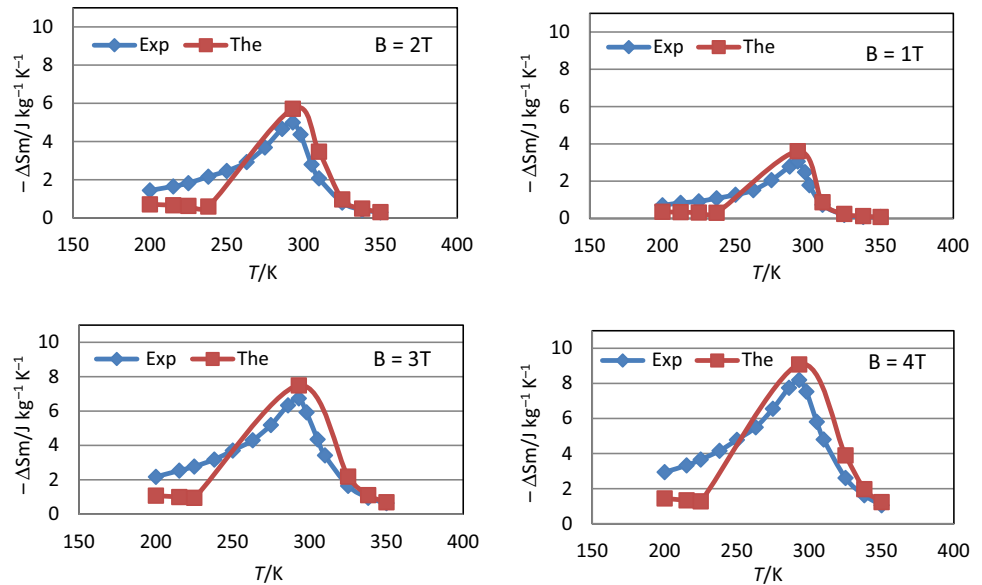
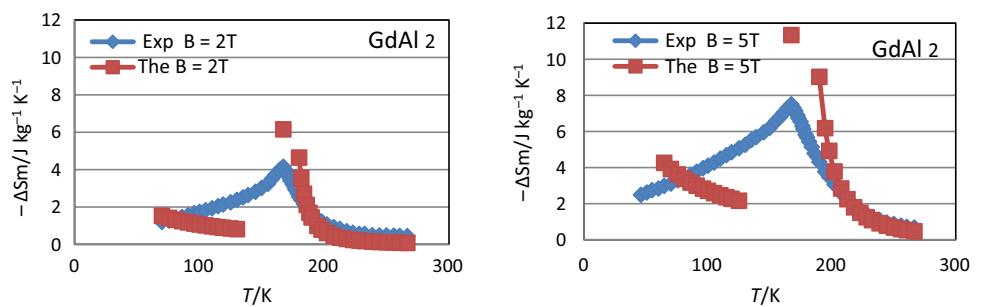


Fig. 5 Comparison of theoretical and experimental values of magnetic entropy as a function of temperature for GdAl₂



$$T_c = 46 \left(G_{\text{Gd}_\alpha \text{R}_{(1-\alpha)}} \right)^{\frac{2}{3}} \quad (33)$$

Validation and discussion

Magnetic entropy

To validate the models, we compared the values found by these models with experimental values from the literature. Figure 4 compares theoretical and experimental values of magnetic entropy as a function of temperature for gadolinium. Experimental values are taken from [35–39]. The figure shows that the variations between experimental and theoretical values are in good agreement only in the paramagnetic phase. Coincidence is not good in the ferromagnetic state, and the difference increases with a

growing magnetic field. At T_c , the coincidence between theoretical and experimental values is high. This finding can be explained by the fact that a paramagnetic material has no spontaneous magnetization; However, under the effect of an external magnetic field, it acquires a magnetization in the same direction as the applied magnetic field. For temperatures $T \ll T_c$, the theoretical values do not coincide with the experimental ones. The non-coincidence can be explained by the fact that temperatures between 200 and 280 K are not much lower than T_c , and the model is no longer applicable in this temperature range. For $T \geq T_c$, the relative error between model-calculated and experimental values is 15% for $B = 1\text{T}$, 12% for $B = 2\text{T}$, 10% for $B = 3\text{T}$, and 9% for $B = 4\text{T}$.

Figure 5 compares theoretical and experimental values of magnetic entropy [35] as a function of temperature for GdAl₂.

Fig. 6 Comparison of theoretical and experimental values of magnetic entropy as a function of temperature for Gd_{0.7}Tb_{0.3}

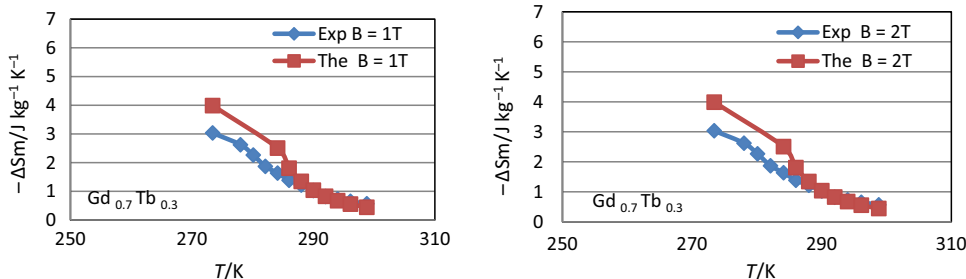


Fig. 7 Comparison of theoretical and experimental values of magnetic entropy as a function of temperature for Gd_{0.87}Dy_{0.13}

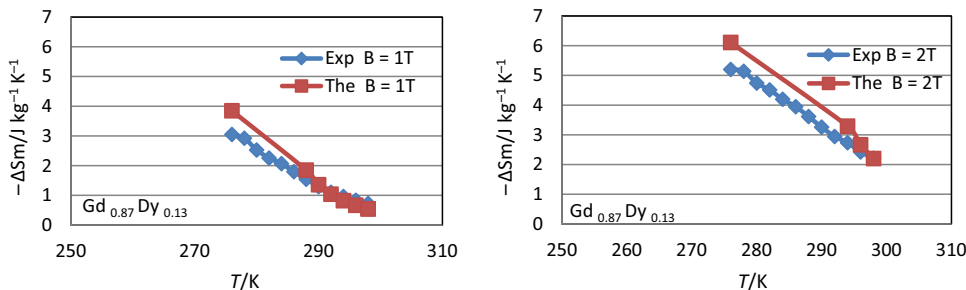


Table 1 Magnetic entropy variation expressions

Temperature/K	Magnetic entropy variation/J kg ⁻¹ K ⁻¹
$T \ll T_c$	$\Delta S_m = \left(\frac{Ng\mu_B B_{max}}{T} + k_B N \right) \left(e^{\frac{-g\mu_B B_{max}}{k_B T}} - 1 \right)$ (Our approach)
$T < T_c$	$\Delta S_m = \left(-a \left(\frac{M_i - M_f}{2} \right) \text{sech}^2(a(T_c - T)) + b \right) B_{max}$ (Semi-empirical method [42–44])
$T \cong T_c$	$\Delta S_m = -1.07 N k_B \left(\frac{g\mu_B J B}{k_B T_c} \right)^{2/3}$ (Theoretical model [34])
$T > T_c$	$\Delta S_m = -\frac{Ng^2 \mu_B^2 J(J+1) B_{max}^2}{6k_B (T - T_c)^2}$ (Our approach)
$T \gg T_c$	$\Delta S_m = -\frac{N(g\mu_B)^2 (J+1) J B_{max}^2}{6KT^2}$ (Our approach)

The same applies to GdAl₂ and Gd at temperatures above the T_c ; Thus, the model is valid. But for $T = T_c$, there is a difference between the theoretical model and the experimental values, in contrast to the results found with Gd, Fig. 4. This difference increases with the applied magnetic field. We can therefore say that the Oesterreicher equation is valid if the temperature T_c of the material is close to room temperature and the magnetic field is not very high. For $T < T_c$, there is no coincidence. In the molecular field model, material magnetization can be described using the Brillouin function, which

is no longer applicable for ferromagnetic states. In the remainder of this work, we focus on temperatures above T_c . We applied the model for the alloys Gd_{0.7}Tb_{0.3} and Gd_{0.87}Dy_{0.13}. The results of the calculations are shown in Figs. 6 and 7. The curves are limited to the models with $T \geq T_c$. We note that the theoretical models fit the experimental ones [40, 41]. Thus, we found that the models are equally applicable for Gd_{0.7}Tb_{0.3} and Gd_{0.87}Dy_{0.13}.

Five magnetic entropy expressions are determined: for $T \ll T_c$, $T < T_c$, $T \cong T_c$, $T > T_c$, and $T \gg T_c$. Comparison with experimental values has shown that three models are valid for $T \ll T_c$, $T > T_c$, and $T \gg T_c$. For temperatures such as $T < T_c$, we verified that the semi-empirical method was the most suitable [42–44]. Moreover, for temperatures such as $T \cong T_c$, theoretical modeling is the most suitable [28, 35]. Table 1 lists the established magnetic entropy models.

Magnetocaloric effect

According to Eq. 25, we can deduce the expression for the magnetocaloric effect (ΔT_{ad}). The comparison between theoretical and experimental values of the magnetocaloric effect [39] as a function of temperature for $T \geq T_c$ for gadolinium is depicted in Fig. 8. Note the agreement of the model with the experimental values for this temperature range.

Fig. 8 Comparison between theoretical and experimental values of the magnetocaloric effect as a function of temperature for $T \geq T_c$ for gadolinium

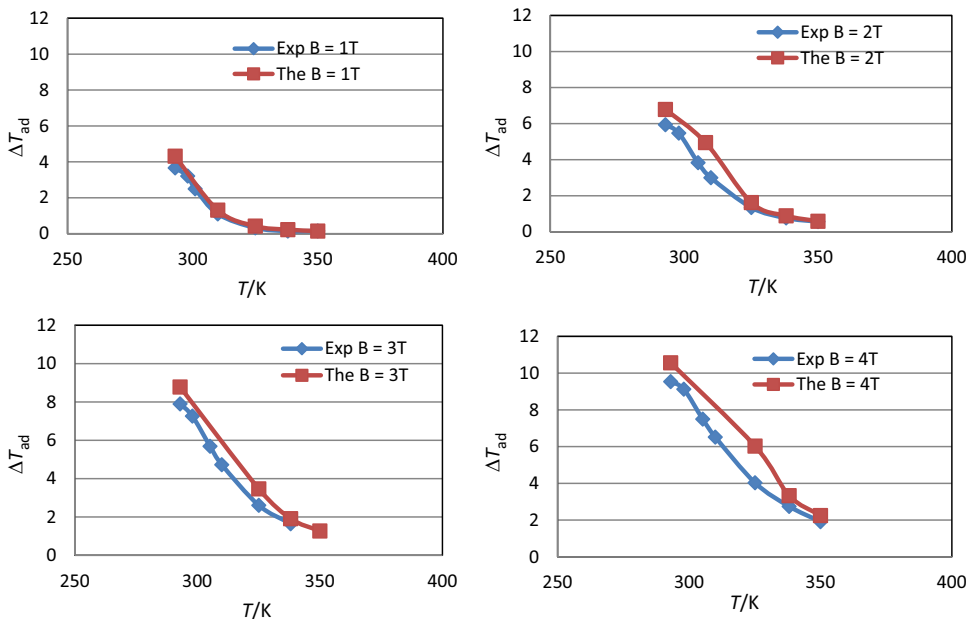


Table 2 Expressions of magnetocaloric effect

Temperature/K	Magnetocaloric effect
$T \ll T_c$	$\Delta T_{ad} = -\frac{T}{C_B} \left(\frac{N g \mu_B B}{T} + k_B N \right) \left(e^{\frac{-g \mu_B B}{k_B T}} - 1 \right)$
$T < T_c$	$\Delta T_{ad} = -\frac{T}{C_B} \left(-a \left(\frac{M_i - M_f}{2} \right) \text{sech}^2(a(T_c - T)) + b \right) B$
$T \cong T_c$	$\Delta T_{ad} = \frac{T}{C_B} 1.07 N k_B \left(\frac{g \mu_B J B}{k_B T_c} \right)^{2/3}$
$T > T_c$	$\Delta T_{ad} = \frac{T}{C_B} \frac{N g^2 \mu_B^2 J(J+1) B^2}{6 k_B (T - T_c)^2}$
$T \gg T_c$	$\Delta T_{ad} = \frac{-N \left(\frac{g \mu_B}{k_B} \right)^2 (J+1) J B^2}{6 C_B K T}$

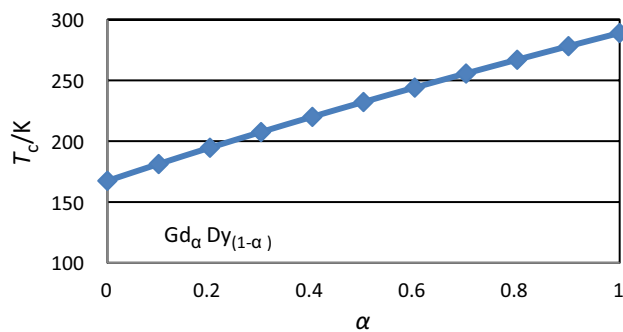


Fig. 10 Variation of T_c as a function of gadolinium concentration in alloys $Gd_\alpha Dy_{(1-\alpha)}$

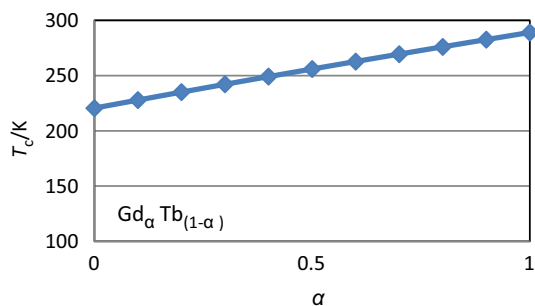


Fig. 9 Variation of T_c as a function of the gadolinium concentration in the alloys $Gd_\alpha Tb_{(1-\alpha)}$

Table 2 lists the established magnetocaloric effect models for each temperature range.

Having shown that the theoretical model is valid for temperatures equal to or higher than the material's T_c , we can apply it to determine a material's T_c and magnetocaloric effect.

Exploitation of validated models

Curie temperature modeling

By exploiting the theoretical model, the T_c can be determined as a function of the concentration α of gadolinium (Figs. 9 and 10).

Smoothing the curve gives us a model of T_c as a function of the α concentration of gadolinium as follows:

- For $Gd_\alpha Tb_{(1-\alpha)}$ ($B = 1T$):

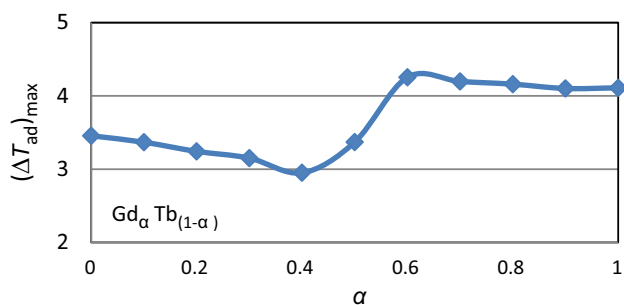


Fig. 11 Variation of $(\Delta T_{ad})_{max}$ as a function of gadolinium concentration in $Gd_{\alpha}Tb_{(1-\alpha)}$ alloy ($B=1T$)

$$T_c(\alpha) = 68.40\alpha + 221.29 (R^2 = 0.99) \tag{34}$$

- For $Gd_{\alpha}Dy_{(1-\alpha)}$ ($B=1T$):

$$T_c(\alpha) = 121.21\alpha + 170.06 (R^2 = 0.99) \tag{35}$$

Modeling of the maximum magnetocaloric effect

When sizing a regenerator of a magnetic refrigeration system, a material is chosen such that its magnetocaloric effect is maximal. Therefore, using the previous theoretical model, we can determine gadolinium concentration α in $Gd_{\alpha}R_{(1-\alpha)}$ alloy to have a desired magnetocaloric effect. The magnetocaloric effect at the material's T_c $(\Delta T_{ad})_{max}$ as a function of gadolinium concentration α in $Gd_{\alpha}Tb_{(1-\alpha)}$ alloy and $(\Delta T_{ad})_{max}$ as a function of gadolinium α concentration in $Gd_{\alpha}Dy_{(1-\alpha)}$ alloys are shown in Figs. 11 and 12, respectively. Smoothing the curve gives us two models of $(\Delta T_{ad})_{max}$ as a function of the concentration α of gadolinium as follows:

- For $Gd_{\alpha} Tb_{(1-\alpha)}$ ($B=1T$):

$$(\Delta T_{ad})_{max} = 96.85\alpha^5 - 248.40\alpha^4 + 214.81\alpha^3 - 68.15\alpha^2 + 5.58\alpha + 3.42 (R^2 = 0.92) \tag{36}$$

- For $Gd_{\alpha} Dy_{(1-\alpha)}$ ($B=1T$):

$$(\Delta T_{ad})_{max} = 1.42\alpha^2 - 1.99\alpha + 4.65 \quad (R^2 = 0.97) \tag{37}$$

Using models to select an active material

Magnetic refrigeration is based on the magnetocaloric effect, an intrinsic property of magnetic materials, which results in the heating or cooling of the material when it is

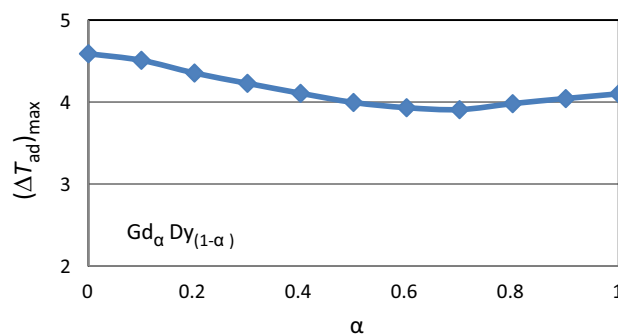


Fig. 12 Variation of $(\Delta T_{ad})_{max}$ as a function of gadolinium concentration in $Gd_{\alpha}Dy_{(1-\alpha)}$ alloy ($B=1T$)

adiabatically magnetized or demagnetized. This phenomenon is maximal when the temperature of the material is equal to its T_c . Consequently, for the cooling system to be effective, the material must be chosen so that its T_c is close to the operating temperature (so that the magnetocaloric effect is at its maximum and the amount of heat transferred is significant). The flow chart in Fig. 13 gives a method for the correct selection of the regenerator's magnetic material to be used in the refrigeration system. This method is not applicable to $Gd_{\alpha} R_{(1-\alpha)}$ but is general for all materials at temperatures close to their T_c . This method enables the selection of the material to be used for the regenerator in a magnetic refrigeration system.

Sizing a multilayer magnetic regenerator

The principle of magnetic refrigeration is based on the magnetocaloric effect. The material is only active if its temperature is equal to the Curie transition temperature (Fig. 1). According to previous numerical studies, the regenerator temperature is not equal to the material temperature T_c , but the profile is linear (Fig. 3). Accordingly, only one layer of the magnetic regenerator is active, and the rest of the regenerator, where temperatures are different at T_c , is not active. Therefore, to improve the efficiency of the magnetic refrigerator, we use a multi-layer regenerator (several layers of different materials) and each layer i is at the T_{ci} of the material of which it is composed.

The flowchart in Fig. 14 details the various steps involved in sizing a multi-layer regenerator used to cool any fluid.

Fig. 13 Method for selecting magnetic materials

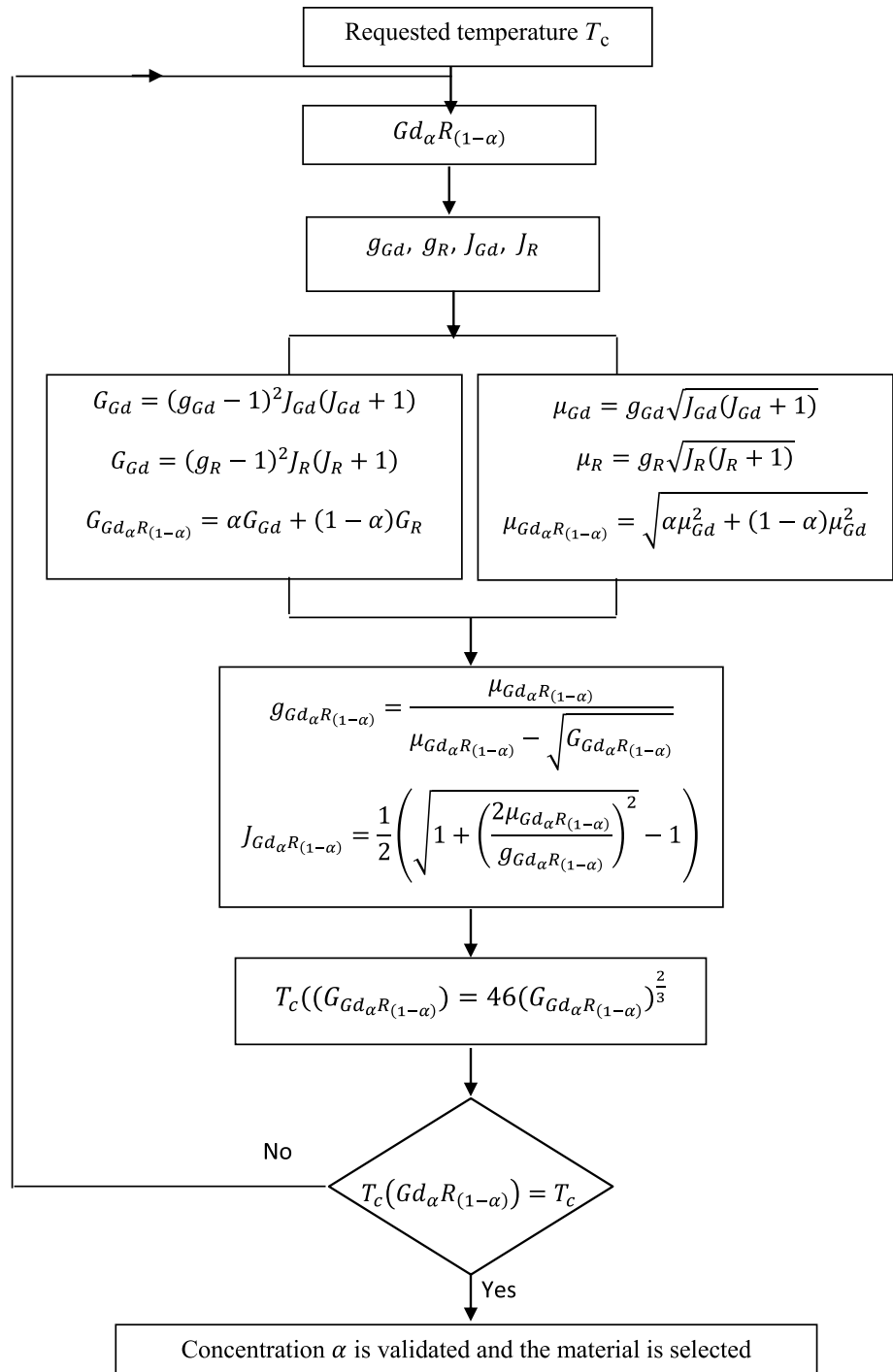
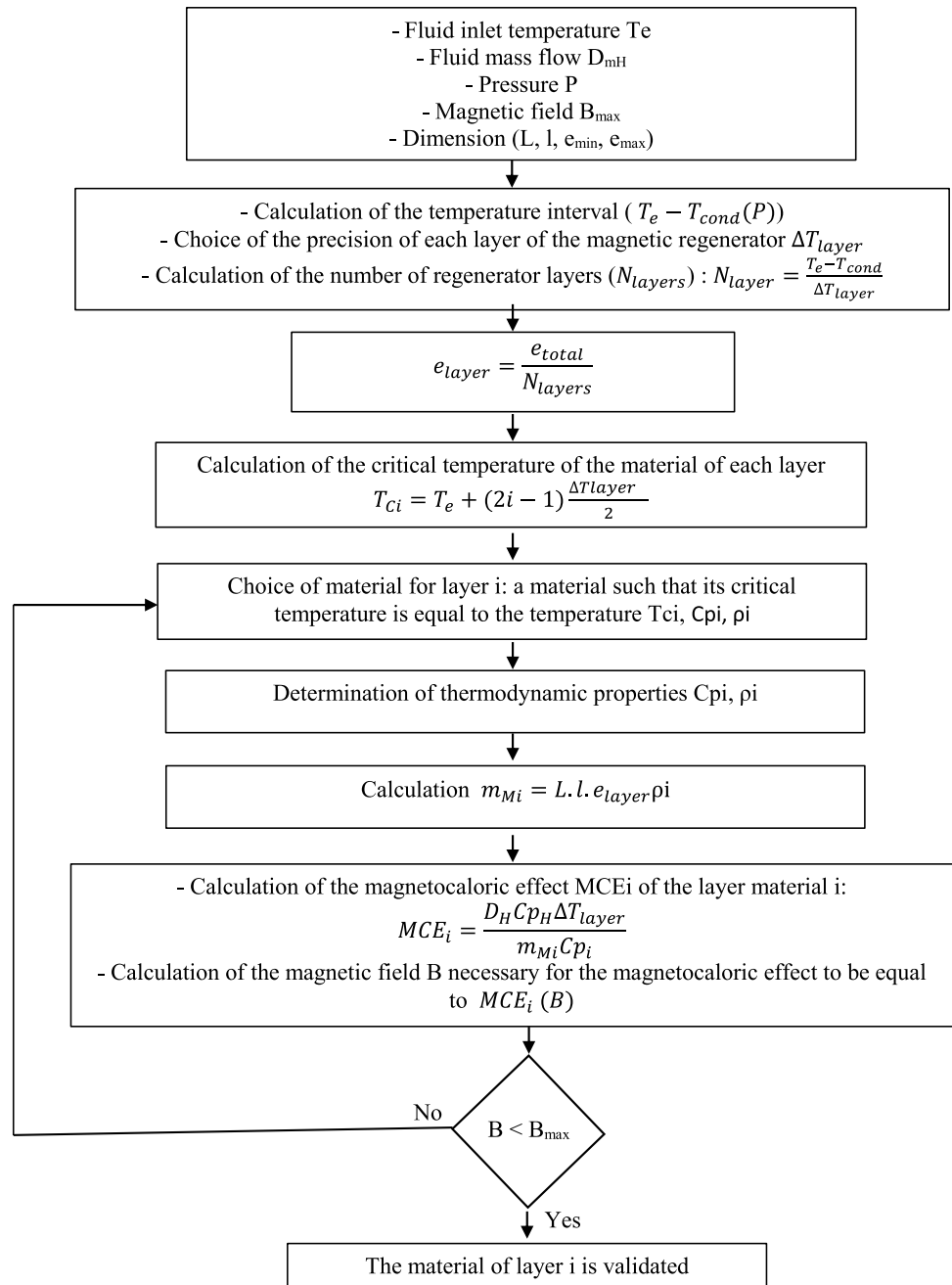


Fig. 14 Method for sizing a multilayer magnetic regenerator



Conclusions

In this work, we proposed a theoretical model of magnetic entropy for each temperature range, as well as for the magnetocaloric effect. Comparisons with the experimental values were carried out to investigate the validity of these models. The conclusion drawn is that these theoretical approaches are valid for paramagnetic states. Oesterreicher's expression for the magnetic entropy near T_c is valid when T_c is close to room temperature and a relatively low magnetic field. The most useful and validated models for an engineer to dimension a magnetic refrigeration system are the expressions for the magnetocaloric effect of a material:

- For $T = T_c$: $\Delta T_{ad} = \frac{T}{C_B} 1.07 N k_B \left(\frac{g \mu_B J B}{k_B T_c} \right)^{2/3}$
- For $T > T_c$: $\Delta T_{ad} = \frac{T}{C_B} \frac{N g^2 \mu_B^2 J(J+1) B^2}{6 k_B (T - T_c)^2}$

The T_c as a function of gadolinium concentration α in a $Gd_\alpha R_{(1-\alpha)}$ is given by:

- For $Gd_\alpha Tb_{(1-\alpha)}$ ($B = 1T$): $T_c(\alpha) = 68.40\alpha + 221.29$
- For $Gd_\alpha Dy_{(1-\alpha)}$ ($B = 1T$): $T_c(\alpha) = 121.21\alpha + 170.06$

These models facilitate the sizing of regenerators for magnetic refrigeration systems. The flowchart of a calculation code based on a new method for choosing the appropriate regenerator material for a magnetic refrigeration system is presented. Another flowchart of an original method and its steps for sizing a multilayer magnetic regenerator is detailed.

In future work, we will choose the heat transfer fluid suitable for a well-defined application.

References

1. Coulomb D. Further limits on HCFCs. *Int J Refrig.* 2007;30:1–2.
2. Söderholm P. The green economy transition: the challenges of technological change for sustainability. *Sustain Earth.* 2020;3(6):2–11.
3. Coulomb D. The carbon impact of the cold chain. *Int J Refrig.* 2021;126:vi–vii.
4. Zina M, Bchiri D, Chrigui M, Jeday MR. A study of the performance coefficient of an active magnetic regenerative refrigeration. *Refrig Sci Technol.* 2016;27:51–4.
5. Barclay JA, Steyert WA. Materials for magnetic refrigeration between 2 K and 20 K. *Cryogenics.* 1982;22:73–80.
6. Foldeaki M, Chahine R, Gopal BR, Bose TK. Effect of sample preparation on the magnetic and magnetocaloric properties of amorphous $Gd_{70}Ni_{30}$. *J Appl Phys.* 1998;83:2727–34.
7. Steyert WA. Stirling cycle rotating magnetic refrigerators and heat engines for use near room temperature. *J Appl Phys.* 1978;49:1216–26.
8. Barclay JA. The theory of an active magnetic regenerative refrigerator. In: *Proceedings of the second biennial conference on refrigeration for cryocooler sensors and electronic systems.* In: NASA conference publication, vol. 2287. 1983, pp. 375–387.
9. Zhang H, Sun YJ, Niu E, Yang LH, Shen J, Hu FX, Sun JR, Shen BG. Large magnetocaloric effects of $RFeSi$ ($R = Tb$ and Dy) compounds for magnetic refrigeration in nitrogen and natural gas liquefaction. *Appl Phys Lett.* 2013;103:2024121–5.
10. Sikora M, Bajorek A, Chrobak A, Deniszczak J, Ziółkowski G, Chełkowska G. Magnetic properties and the electronic structure of the $Gd_{0.4}Tb_{0.6}Co_2$ compound. *Materials.* 2020;13:5481.
11. Lebouc A, Almanza M, Yonnet JP, Legait U, Roudaut J. Refrigeration magnetique Etat de l'art et developpements recents. In: *Symposium de genie electrique.* 2014.
12. Meddeb Z. Modelling of active magnetic regenerative refrigeration system performance by new approaches. In: *Advances in the modelling of thermodynamique edition.* IGI Global; 2022, pp. 168–191, ISBN13: 9781799888017.
13. Al-Kouz W, Abderrahmane A, Shamshuddin M, et al. Heat transfer and entropy generation analysis of water– Fe_3O_4 /CNT hybrid magnetic nanofluid flow in a trapezoidal wavy enclosure containing porous media with the Galerkin finite element method. *Eur Phys J Plus.* 2021;136:1184.
14. Barnoon P, Toghraie D, Karimipour A. Application of rotating circular obstacles in improving ferrofluid heat transfer in an enclosure saturated with porous medium subjected to a magnetic field. *J Therm Anal Calorim.* 2021;145:3301–23.
15. Barnoon P, Toghraie D, Salarnia M, et al. Mixed thermomagnetic convection of ferrofluid in a porous cavity equipped with rotating cylinders: LTE and LTNE models. *J Therm Anal Calorim.* 2021;146:187–226.
16. Mousavi SM, Biglarian M, Darzi AAR, et al. Heat transfer enhancement of ferrofluid flow within a wavy channel by applying a non-uniform magnetic field. *J Therm Anal Calorim.* 2020;139:3331–43.
17. Talebizadehsardari P, Shahsavari A, Toghraie D, et al. An experimental investigation for study the rheological behavior of water-carbon nanotube/magnetite nanofluid subjected to a magnetic field. *Physica A.* 2019;534:122–9.
18. Mousavi SM, Darzi AAR, Akbari O, Toghraie D, Marzban A. Numerical study of biomagnetic fluid flow in a duct with a constriction affected by a magnetic field. *J Magn Magn Mater.* 2018;10:043.
19. Ibrahim M, Saeed T, Bani FR, Sedeh SN, Chu Y-M, Toghraie D. Two-phase analysis of heat transfer and entropy generation of water-based magnetite nanofluid flow in a circular microtube with twisted porous blocks under a uniform magnetic field. *Powder Technol.* 2021;384:522–41.
20. Okonkwo EC, Wole-Osho I, Almanassra IW, et al. An updated review of nanofluids in various heat transfer devices. *J Therm Anal Calorim.* 2021;145:2817–72.
21. Afrand M, Sina N, Teimouri H, Mazaheri A, Safaei MR, Esfe MH, Kamali J, Toghraie D. Effect of magnetic field on free convection in inclined cylindrical annulus containing molten potassium. *Int J Appl Mech.* 2015;7:155052.
22. Shah SS, Öztop HF, Ul-Haq R, Abu-Hamdeh N. Natural convection process endorsed in coaxial duct with Soret/Dufour effect. *Int J Numer Methods Heat Fluid Flow.* 2023;33:96–119.
23. Khan Usafzai W, Haq RU, Aly EH. Wall laminar nanofluid jet flow and heat transfer. *Int J Numer Methods Heat Fluid Flow.* 2023;33:1818–36.
24. Soomro FA, Usman M, El-Sapa S, et al. Numerical study of heat transfer performance of MHD Al_2O_3 -Cu/water hybrid nanofluid flow over inclined surface. *Arch Appl Mech.* 2022;92:2757–65.
25. Khan ZH, Usman M, Khan WA, et al. Thermal treatment inside a partially heated triangular cavity filled with casson fluid with an inner cylindrical obstacle via FEM approach. *Eur Phys J Spec.* 2022;231:2683–94.

26. Soomro FA, Hamid M, Hussain ST, et al. Constructional design and mixed convection heat transfer inside lid-driven semicircular cavity. *Eur Phys J Plus*. 2022;137:781.
27. Beltran-Lopez JF, Sazatornil M, Palacios E, et al. Application of simulations to thermodynamic properties of materials for magnetic refrigeration. *J Therm Anal Calorim*. 2016;125:579–83.
28. Tishin AM, Spichkin YI. The magnetocaloric effect and its applications. Bristol and Philadelphia: Institute of Physics Publishing; 2003. (ISBN 0-7503-0922 9).
29. Richard A. Swalin; thermodynamics of solids. Canada: Wiley; 1972.
30. Azad A, Ahmadi P, Geshani H, et al. Parametric study of an active magnetic refrigeration (AMR) system on exergy efficiency and temperature span with Gadolinium. *J Therm Anal Calorim*. 2021;145:1691–710.
31. Barclay JA, Steyert WA. Materials for magnetic refrigeration between 2K and 20 K. *Cryogenics*. 1982;10:73–80.
32. Quinet P, Biémont E. Landé g-factors for experimentally determined energy levels in doubly ionized lanthanides. *At Data Nucl Data Tables*. 2004;87:207–30.
33. Aslani A, Ghahremani M, Zhang M, Bennett LH, Torre ED. Enhanced magnetic properties of yttrium-iron nanoparticles. *AIP Adv*. 2017;7:056423.
34. Smaili A, Chahine R. Thermodynamic investigations of optimum active magnetic regenerators. *Cryogenics*. 1998;38:247–52.
35. Oesterreicher H, Parker FT. Magnetic cooling near Curie temperatures above 300K. *J Appl Phys*. 1984;55:4334.
36. Balli M, Fruchart D, Gignoux D, Miraglia S, Hlil EK, Wolfers P. Modelling of the magnetocaloric effect in $Gd_{1-x}Tb_x$ and MnAs compounds. *J Magn Magn Mater*. 2007;316:e558–61.
37. Digué G, Lin G, Chen J. Impact of the initial field on the thermodynamic performance of room-temperature magnetic refrigeration cycle. *Int J Refrig*. 2013;36:2395–402.
38. Dankov SY, Tishin AM. Magnetic phase transitions and the magnetothermal properties of gadolinium. *Phys Rev B*. 1998;57:3478–90.
39. Risser M, Vasile C, Engel T, Keith B, Muller C. Numerical simulation of magnetocaloric system behaviour for an industrial application. *Int J Refrig*. 2010;33:973–81.
40. du Tremolet de Lacheisserie E. Magnetic properties and critical behaviour of $GdAl_2$: thermal expansion, magnetization, magnetostriction and magnetocaloric effect. *J Magn Magn Mater*. 1988;73:289–98.
41. Ao WQ, Jian YX, Liu FS, Feng XW, Li JQ. The influence of gallium on magnetocaloric effect in $Gd_{60}Tb_{40}$ alloys. *J Magn Magn Mater*. 2006;307:120–3.
42. Hamad MA. Magnetocaloric effect in $La_{1-x}Ce_xMnO_3$. *J Adv Ceram*. 2015;4(3):206–10.
43. Hamad MA. Simulated magnetocaloric properties of $MnCr_2O_4$ spinel. *Process Appl Ceram*. 2016;10:33–6.
44. Hamad MA. Magnetocaloric properties of $La_{0.666}Sr_{0.373}Mn_{0.943}Cu_{0.018}O_3$. *Process Appl Ceram*. 2017;3:225–8.

Publisher's Note Springer Nature remains neutral with regard to jurisdictional claims in published maps and institutional affiliations.

Springer Nature or its licensor (e.g. a society or other partner) holds exclusive rights to this article under a publishing agreement with the author(s) or other rightsholder(s); author self-archiving of the accepted manuscript version of this article is solely governed by the terms of such publishing agreement and applicable law.